Tuning infrared emission from microstrip arrays

W. L. Schaich*
Physics Department, Indiana University, Bloomington, Indiana 47405, USA

Irina Puscasu
FLIR Systems, Billerica, Massachusetts 01862, USA
(Received 7 August 2012; published 21 December 2012)

Earlier work has shown that a narrow-frequency-band, wide-angle emission is produced by an array of metal patches supported on a thin dielectric layer covering a ground plane. The modes responsible for this emission are local plasmons trapped under the metal patches. As the dielectric layer thickness, h_d, is increased, the resonant emission fades in strength because the plasmon modes can no longer be trapped under a single patch. Further increases in h_d, making it comparable to the light wavelength in the dielectric layer, lead to a collection of new emission peaks. These are narrower than the one peak found for small h_d but they are not well separated. We have found that some of these peaks can be suppressed over a narrow range of h_d. This leaves one with well-separated, narrow-band emission peaks. We have identified the physical mechanism for this selective suppression of emission peaks.

DOI: 10.1103/PhysRevB.86.245423 PACS number(s): 78.67.−n, 78.20.Ci, 78.20.Bh, 42.25.Fx

Among the central properties of plasmonic nanostructures are the dispersion relations and excitation probabilities of various plasmon resonances. In this paper, we examine these properties within a special class of nanostructures, probed in a particular way. The structures have three layers as illustrated in Fig. 1. On the bottom is an opaque ground plane of thickness h_f. Since no light can pass through this layer, what supports it is optically irrelevant. On top of the ground plane, there is a uniform dielectric layer of thickness h_d. Finally, the dielectric layer is covered with a two-dimensional (2D) (or one-dimensional) grating made from metal patches (or stripes) of height h_p and various shapes. For instance, the cross section of a patch could be round or rectangular or more complex.

As a probe of these systems, we consider linearly polarized light of wavelength λ incident from the air above the layers. Referring to Fig. 1, the incident light propagates along $+\hat{x}$ and is polarized along $\hat{y}$. We examine the reflection coefficient, R, of exiting light and look for resonant dips in R as a function of λ. We limit our study to long enough wavelengths (or short enough grating periods) so that the only possible reflected beam is along $-\hat{x}$; i.e., so that no diffracted beam can propagate away from the sample. Then, by Kirchoff's law,[1] one has for emission (E), absorption (A), and reflection (R) probabilities,

$$E = A = 1 - R. \tag{1}$$

Hence, a resonant dip in reflection implies a resonant peak in absorption or emission. For various practical applications, one would like the resonances to be strong, narrow, and well separated.

Systems such as those illustrated in Fig. 1 have been often studied (see Refs. 2–31). This list only includes papers where the examined resonances are at wavelengths less than about 10 μm. A simple result is found when h_d is larger than the light's penetration depth in the metal but still much smaller than its wavelength in the dielectric. A sequence of isolated, narrow, resonant dips in R is then possible. These resonances are due to the excitation of transverse electromagnetic (TEM) waves trapped underneath individual metal structures in the top layer. They may be described[4] using the limiting dispersion relation for a microstrip or MIM (metal-insulator-metal) system:

$$\omega = Qc/n_d, \tag{2}$$

where Q is the wave vector in the surface (y-z) plane, n_d is the dielectric's index of refraction, ω is the light's angular frequency, and c is the vacuum speed of light. The resonance locations depend sensitively on the patch (or stripe) shape and dimensions, but weakly on the grating's period. This behavior is due to the resonances' origin in localized, rather than extended, surface plasmons.

Our interest here is with how things change when h_d is increased, becoming comparable with λ/n_d and the grating period. One might expect that the grating would then lose the ability to trap waves underneath its metal patches (or stripes) and instead act to excite standing waves extending along the ground plane. There should also be the possibility of standing waves of variation along $\hat{x}$ within the dielectric. These two types of standing waves, controlled by either a grating period or the dielectric thickness, should interact with each other. Some papers have already considered the behavior in this regime,[2,10,11,16,21,31] but they typically show results for only a few values of h_d or λ. We present a more systematic study that clarifies trends and reveals some surprises.

Our simulations are done using the finite-difference time-domain (FDTD) scheme.[32] The metal is described by the Drude model using the parameters of Ref. 33 for gold, while the dielectric, with silicon dioxide in mind, is assigned the constant, real-valued index of refraction $n_d = 1.45$. This latter approximation suppresses the effect of optical phonons in the dielectric, but since the resonances we find are generally at wavelengths well below 10 μm, the quantitative error is slight.[4] Both the ground plane and the structured layer are given a thickness of $h_p = h_f = 200$ nm. The period of either the 2D square array of patches or the 1D array of stripes is $a = 2$ μm. Our primary calculations are done for round patches of diameter $D = 1$ μm or for rectangular stripes

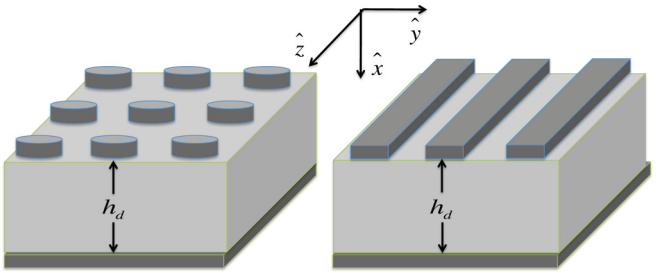

FIG. 1. Sketch of characteristic structures for which response will be calculated. The bottom two layers are uniform and consist of metal for the ground plane and an insulator for the dielectric spacer, respectively. The top metal layer may be a 2D array of patches or a 1D grating of stripes.

of width $w = 0.8$ μm. A simulation is done with the total field/scattered field scheme by sending in a Gaussian pulse with a root mean square width in x of 0.3 μm. Our spatial mesh has $\Delta x = \Delta y = \Delta z = 20$ nm, and the time step is $c\Delta t = 10$ nm.

We allow 12,000 time steps, which is enough to ensure that all significant reflections have occurred. From the results, we can determine the time-Fourier transform of both the incident E_y and the laterally averaged, reflected E_y. The absolute squared ratio of these two transforms gives R.

We begin with Fig. 2 showing results for round patches where the dielectric layer thickness varies from 20 nm to 3 μm. The diffraction (Rayleigh-Wood) threshold is at $\lambda = a$, and we are showing R only for longer wavelengths. The simple result produced by TEM waves trapped under the patches is responsible for the structure around $\lambda = 4$ μm, but it fades away as h_d grows through 0.1 μm. It is replaced by a collection of resonances that smoothly evolve in location and strength with h_d. Before attempting to understand the physical origin of the many new resonances, we draw the reader's attention to the qualitative appearance of the plot. There are wide plateaus of high R separated by narrow valleys of low R, with the

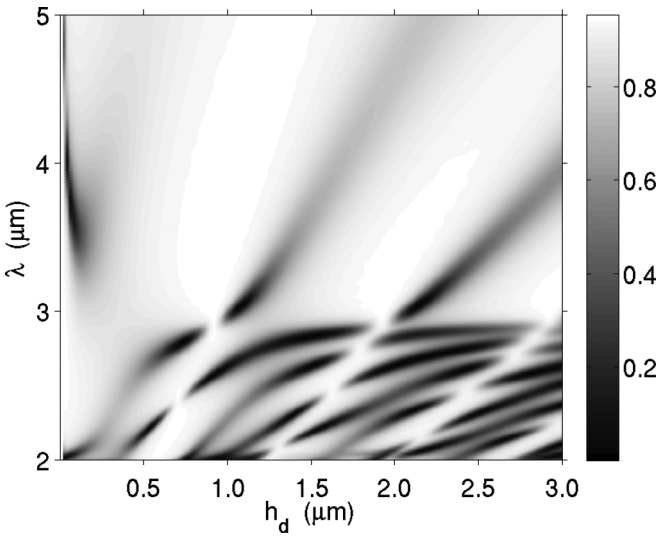

FIG. 2. Reflectivity R for normally incident light as a function of λ and h_d for a 2D square array of round patches. See text for parameter values held fixed.

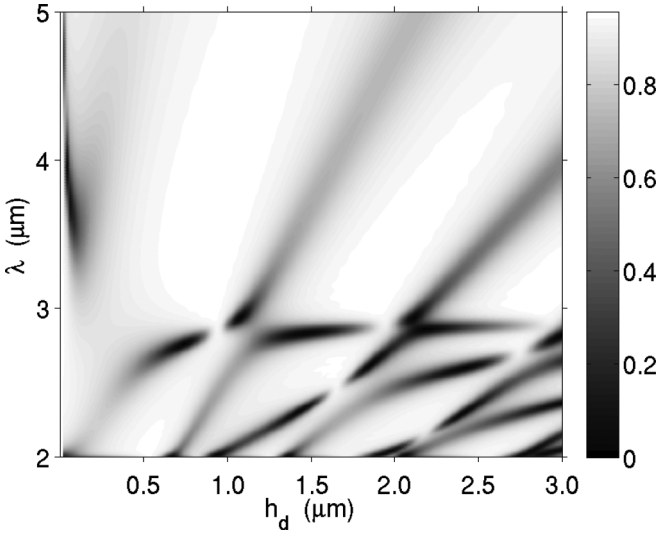

FIG. 3. Reflectivity R for normally incident light as a function of λ and h_d for a 1D grating of stripes of rectangular cross section. See text for parameter values held fixed.

latter representing the h_d dispersion of the resonances. This was expected. The surprising feature is the presence of several bridges of high R that cross over the valleys of low R. These bridges of high R imply that particular resonances can be briefly suppressed as h_d varies. One needs to explain not only the valleys but also the bridges.

These tasks are helped by examining simpler systems. In Fig. 3, we plot results for when patches in the top layer are replaced by stripes of width w (see Fig. 1). The computational effort for these FDTD simulations is considerably reduced since none of the fields will vary with the z-coordinate when the incident light comes in along $\hat{x}$, polarized along $\hat{y}$. Furthermore, only three field components are nonzero: E_x, E_y, and H_z. The reflection spectrum in Fig. 3 is qualitatively similar to that in Fig. 2. There are again plateaus separated by valleys, which are occasionally bridged. One remarkable new feature is that there are fewer resonances for 2 μm $< \lambda <$ 3 μm.

We now turn to still simpler models that will allow (near) analytic estimates of resonance locations. The key simplification is to eliminate the structure in the top layer. We examine two extremes: Either eliminate the top layer completely, or replace it with a uniform metal layer. In the former case, we end up with a dielectric waveguide, while in the latter case, we have an MIM plasmonic waveguide. We analyze these two possibilities in slightly different ways.

For the plasmonic waveguide, we ignore the imaginary part of the metal's dielectric function, imagine the two metal layers are semi-infinite, and then calculate the dispersion of freely propagating modes with surface-parallel wave vector $\boldsymbol{Q} = Q\hat{y}$. For modes with transverse magnetic (TM) polarization, the modes' locations are solutions of the transcendental equations[34]

$$\overline{p}_m/\varepsilon_m = \pm p_d \tan^{\pm 1}(p_d h_d/2)/\varepsilon_d, \tag{3}$$

where

$$p_d = (\omega^2 \varepsilon_d/c^2 - Q^2)^{1//2} \tag{4}$$

and

$$\overline{p}_m = (Q^2 - \omega^2 \varepsilon_m / c^2)^{1/2}. \quad (5)$$

Here, ε_m or ε_d is the dielectric function of the metal or dielectric, respectively. The upper or lower signs in Eq. (3) are for modes for which H_z (and E_x) field components are even or odd, respectively, about the midpoint (along $\hat{x}$) of the dielectric layer. Above the dielectric light line, defined by $p_d = 0$ [or Eq. (2)], the modes are standing waves of motion in the dielectric for which parity jumps between $+1$ and -1 as ω increases. Since the bulk plasmon energy is far above our range of interest, we do not consider how things change when $\overline{p}_m$ becomes imaginary. However, we do examine possible modes beneath the dielectric light line where $p_d \to \bar{p}_d = (Q^2 - \omega^2 \varepsilon_d / c^2)^{1/2}$ and Eq. (4) becomes

$$\bar{p}_m / \varepsilon_m = -\bar{p}_d \tanh^{\pm 1}(\bar{p}_d h_d / 2) / \varepsilon_d. \quad (6)$$

The lowest energy mode at any Q has even $H_z$and always obeys Eq. (6). The next lowest mode has odd H_z and crosses the dielectric light line, going from a solution of Eq. (4) to a solution of Eq. (6) as Q increases. All higher-energy modes exist only above the dielectric light line.

The collection of mode dispersions is plotted in Fig. 4 for two different choices of h_d. Note how the mode frequencies at any Q shift downward as h_d increases. Hence, in a fixed frequency range, the number of modes increases as h_d increases. This qualitative behavior is also evident in Figs. 2 and 3 for $2\ \mu\text{m} < \lambda < 3\ \mu\text{m}$. For more transparency, we remark that for the relatively small values of ω and Q examined here, the modes are fairly well described by

$$\omega^2 \varepsilon_d / c^2 = (m\pi / h_d)^2 + Q^2 \quad (7)$$

with $m = 0, 1, 2, \ldots$.

Consider next the response of a planar dielectric waveguide, the cladding of which consists of semi-infinite metal and vacuum. We again ignore the imaginary part of the metal's dielectric function, so we can determine mode dispersions. However, instead of writing out field profiles in the three separate regions and matching across boundaries, we imagine a reflection problem where the incident TM wave comes from the vacuum on top. We constrain Q and ω so one is below the vacuum light line, $\omega = Qc$, and look for singularities in r_{123}, the reflection amplitude.[35] Here, the subscripts label the three regions vacuum, dielectric, and metal as 1, 2, and 3, respectively, and we find r_{123} from the Airy formula[36]

$$r_{123} = (r_{12} + r_{23} e^{2ip_2 h_2}) / (1 - r_{23} r_{21} e^{2ip_2 h_2}), \quad (8)$$

where $h_2 = h_d$, and the single interface reflection amplitudes are

$$r_{ij} = (\varepsilon_j p_i - \varepsilon_i p_j) / (\varepsilon_j p_i + \varepsilon_i p_j) = -r_{ji}, \quad (9)$$

with $p_i^2 = \omega^2 \varepsilon_i / c^2 - Q^2 = -\overline{p}_i^2$. By design, one has $\overline{p}_1$ and $\overline{p}_3$ real valued so that the modes decay away from the dielectric layer. All but one of the modes begin at nonzero Q on the vacuum light line and move as Q increases down towards the dielectric light line. The lowest energy mode starts at $\omega = 0 = Q$ and crosses over the dielectric light line at a nonzero value of Q, becoming the surface plasmon of an (isolated) dielectric/metal interface as $Q \to \infty$.

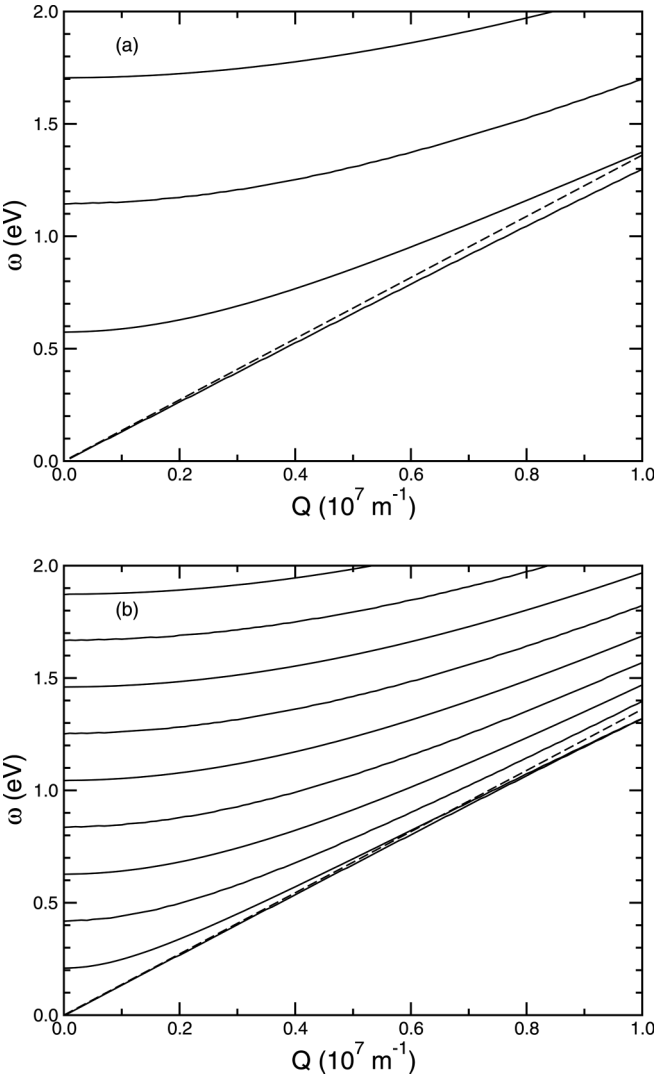

FIG. 4. Dispersion of TM modes of a MIM waveguide. The physical properties of the metal and insulator are the same as those used in Figs. 2 and 3, except that the imaginary part of the Au dielectric function has been set to zero. The bulk plasmon energy is off scale at 2.96 eV. The dashed line is the dielectric light line. In (a) $h_d = 0.7\ \mu$m and in (b) $h_d = 2\ \mu$m.

The collection of mode dispersions is plotted in Fig. 5 for the same two choices of h_d as in Fig. 4. In a fixed frequency range, say between the two light lines, we again see that the number of modes increases as h_d increases. There are several technical points to note about the scheme based on Eq. (8) for finding modes. One is essentially looking for a zero in the denominator of r_{123}. Indeed, if we assume layers 1 and 3 are identical, the vanishing of the denominator in Eq. (8) is algebraically equivalent to Eqs. (3) or (6). Second, the numerical solution requires special care near the dielectric light line, since when $p_2 = 0$, it implies that $r_{2i} = -1$ for $i \neq 2$ and hence $r_{123} = 0/0$. Third, one can also do the calculation if the dielectric functions have imaginary parts. Since $\text{Im}(\varepsilon_m) \ll |\text{Re}(\varepsilon_m)|$ in our frequency range of interest, we find a sharp peak (but not a singularity) in r_{123} as ω is varied over real values at fixed, real Q. The locations of such peaks are close to where r_{123} is singular when $\text{Im}(\varepsilon_m) = 0$.

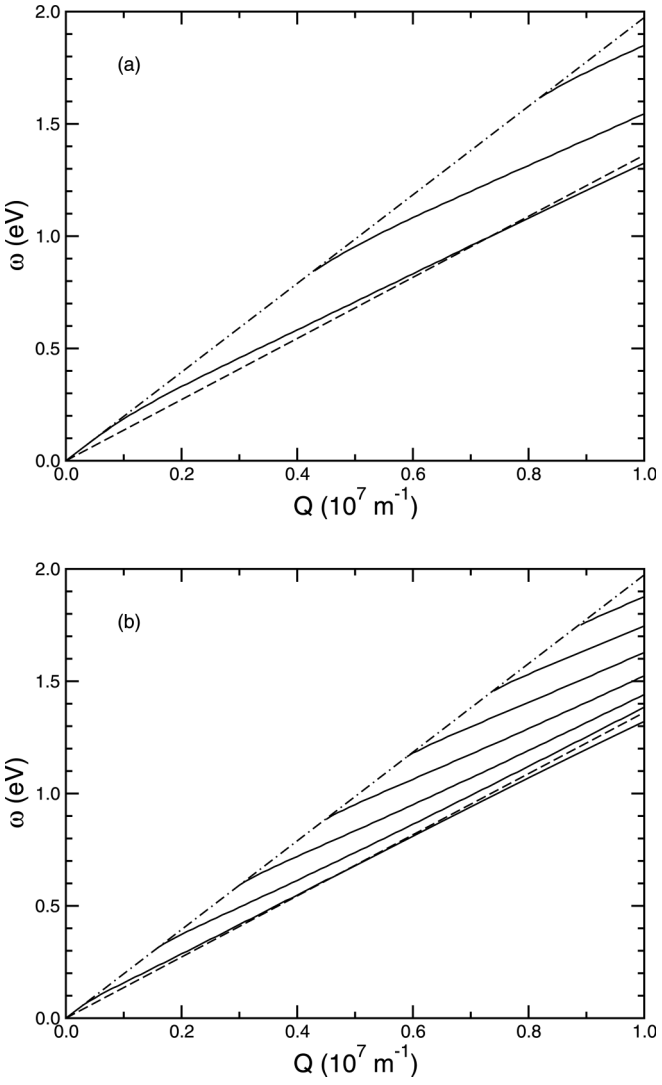

FIG. 5. Dispersion of TM modes of a dielectric waveguide. The physical model is the same as for Fig. 4, except that the top metal layer is absent. The dashed line is the dielectric light line, while the dotted-dashed line is the vacuum light line. In (a) $h_d = 0.7$ μm and in (b) $h_d = 2$ μm.

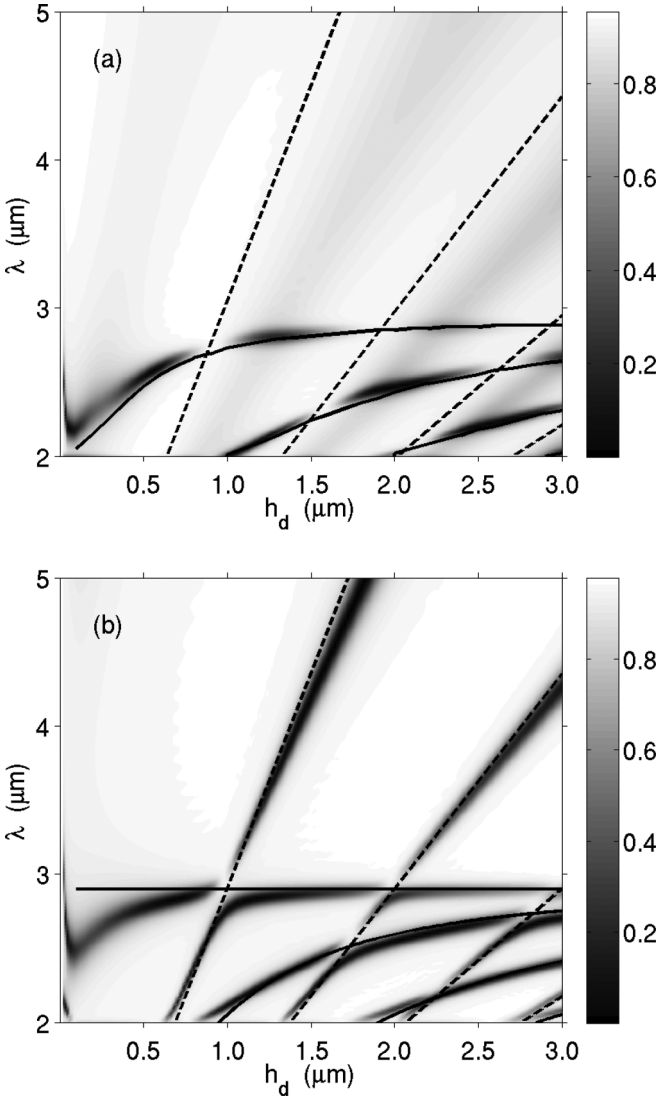

FIG. 6. Comparison of dispersion of waveguide modes with simulated reflectivity spectra of 1D grating arrays of stripes. In (a) $w = 0.4$ μm, and the TM modes of a dielectric waveguide at $Q = 2\pi/a$ are drawn as solid lines. The dashed lines are from Eq. (10) using $\delta = 50$ nm. In (b) $w = 1.6$ μm, and the TM modes of a MIM waveguide at $Q = 2\pi/a$ are drawn as solid lines. The dashed lines are from Eq. (10) with $\delta = 0$.

In order to compare the results of Figs. 4 and 5 with the simulations of Figs. 2 or 3, we set $Q = 2\pi/a$ and plot wavelength $\lambda = 2\pi c/\omega$ versus h_d. It is with this choice of Q that we make contact with our physical system that has a structured top layer. Initially, we are not addressing how the waveguide modes could actually be excited; instead, we are merely examining how they disperse with h_d if excited. To aid the comparison, we first consider 1D gratings with suitable choices of stripe width w, either close to zero or close to a. The former case has the top layer nearly absent and should compare well with the dielectric waveguide modes, while for the latter case, the top layer is nearly uniform and should compare well with the MIM plasmonic modes.

The comparisons are shown in Fig. 6. They are quite favorable over the range $2\ \mu\text{m} < \lambda < 3\ \mu\text{m}$, especially for the $w = 0.4$ μm case, which we discuss first. The FDTD simulations again show narrow valleys of low R, interrupted by bridges of high R. Compared to Fig. 3, the structure at small h_d due to a plasmon trapped under a stripe occurs at a much smaller λ due to the smaller stripe width. This resonance's location should not (and does not) match with waveguide modes at $Q = 2\pi/a$. Along the dispersion curve of any one resonance, its excitation strength (as indicated by its $A = 1 - R$) oscillates in size as h_d varies. Since these resonances can only be excited by scattering from the stripes, it is appealing to associate large A with strong scattering and vice versa. This association suggests a way to explain the bridges of high R. In the absence of the top layer, light at normal incidence will strongly reflect from the ground plane but be mostly transmitted through the air/dielectric interface. This will lead to a standing wave for E_y as a function of the normal coordinate x. Hence, as h_d is varied, the amplitude of E_y on the top of the dielectric layer will oscillate in magnitude.

Now introduce a top layer of narrow stripes. If we assume that the E_y amplitude in their absence determines how strongly the stripes can scatter the light into nonzero Q variations, then we can predict when this scattering should be strong or weak. In particular, weak scattering should occur when

$$m\lambda/2 = n_d(h_d + \delta), \tag{10}$$

where m is an integer, and δ is a fudge parameter to account for the fact that the stripes have a nonzero thickness on top of the dielectric layer. The straight lines of Eq. (10) are also included in Fig. 6(a) with the choice of $\delta = 50$ nm, a reasonable value since $h_p = 200$ nm. They pass through every one of the bridges of high R. We stress that the stripe width does not explicitly appear in Eq. (10), so its prediction will be checked for other choices of w.

We next turn to Fig. 6(b), which compares a simulation using $w = 1.6$ μm with the modes of a MIM waveguide. The mode dispersions of the MIM waveguide are quite similar to those of the dielectric waveguide, except for the lowest-energy mode, which for the MIM has approximately [from Eq. (7)] $\lambda = n_d a = 2.9$ μm. The simulation results do not show as strong a difference between $w = 1.6$ μm and $w = 0.4$ μm. As an aside, we remark that the structure at the smallest h_d in Fig. 6(b) is due to a higher-order (third) trapped mode. The lowest-order trapped mode is located off scale near 7 μm, and the second cannot be excited with normal incidence. The simulation results in Fig. 6(b) show additional resonances that exhibit avoided crossings with MIM modes at $Q = 2\pi/a$. These may be associated with $Q = 0$ MIM modes, which from Eq. (7) obey $\lambda = 2n_d h_d/m$; i.e., Eq. (10) with $\delta = 0$. These straight-line dispersions reasonably track the additional resonances. They also pass close to the bridges of high R, which now appear near the avoided crossings between $Q = 0$ and $Q = 2\pi/a$ resonances. Evidence for $Q = 0$ resonances is barely visible in Fig. 6(a), but more so in Figs. 2 and 3. However, the slope of their straight-line dispersion does not match the MIM predictions.

In Fig. 7, we compare mode estimates with the FDTD simulation results of Fig. 3. Since $w = 0.8$ μm is neither a small nor a large fraction of our $a = 2$ μm, we should not expect as good agreement as found in Fig. 6. However, it still appears that each resonance seen in the simulations can be associated with either a $Q = 2\pi/a$ or $Q = 0$ mode, although the wavelengths of the latter are systematically lower in the simulations. The efficacy of Eq. (10) for locating bridges of high R remains good.

Finally, we come back to Fig. 2 with the 2D array of patches in the top layer. Here, there are clearly more resonances than waveguide modes that we have so far identified. The resonances already used have Q being either zero or the shortest reciprocal lattice vector of the array, $2\pi/a$. Allowing for scattering to $Q = 4\pi/a$ would from Eq. (7) produce modes at wavelengths less than $n_d a/2 = 1.45$ μm; i.e., below the Rayleigh-Wood threshold of 2 μm. For this reason, we did not consider this possibility when discussing Figs. 6 and 7. With a 2D array of patches, we have more choices of reciprocal lattice vectors. One possibility is $\boldsymbol{Q} = (\hat{y} + \hat{z})2\pi/a$, along with its three symmetric equivalents. However,its magnitude is $Q = 2\sqrt{2}\pi/a$, which leads to modes of wavelength less

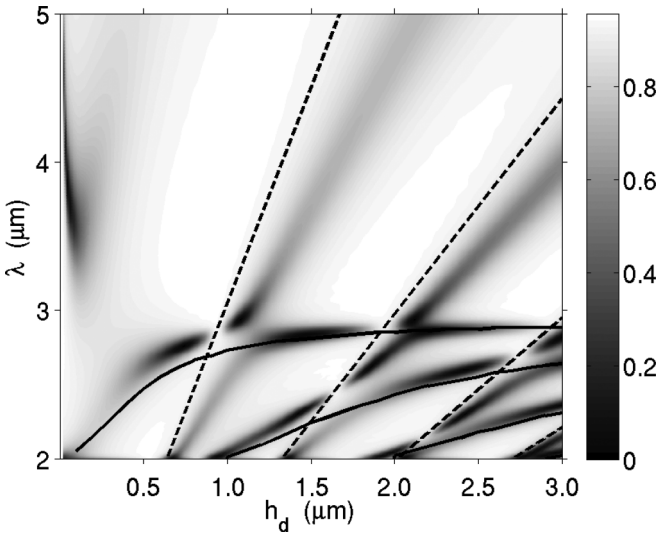

FIG. 7. Comparison of dispersion of TM dielectric waveguide modes with the reflectivity spectra of Fig. 3. The modes at $Q = 2\pi/a$ are drawn as solid lines. The dashed lines are from Eq. (10) using $\delta = 50$ nm.

than $n_d a/\sqrt{2} = 2.05$ μm, which are also too short to account for the results in Fig. 2. Another possibility is to consider $\boldsymbol{Q} = \pm\hat{z}2\pi/a$, which can produce modes with wavelengths significantly above a. If we assume these have the same polarization as the incident light, then we should include transverse electric (TE) modes in the waveguide estimates. In terms of the approach based on singularities in the reflection amplitude of Eq. (8), we only need to change the single interface reflection amplitudes to

$$r_{ij} = (p_i - p_j)/(p_i + p_j) = -r_{ji}. \tag{11}$$

Again we find a sequence of waveguide modes. In Fig. 8, we have plotted the TM and TE modes at $Q = 2\pi/a$ for

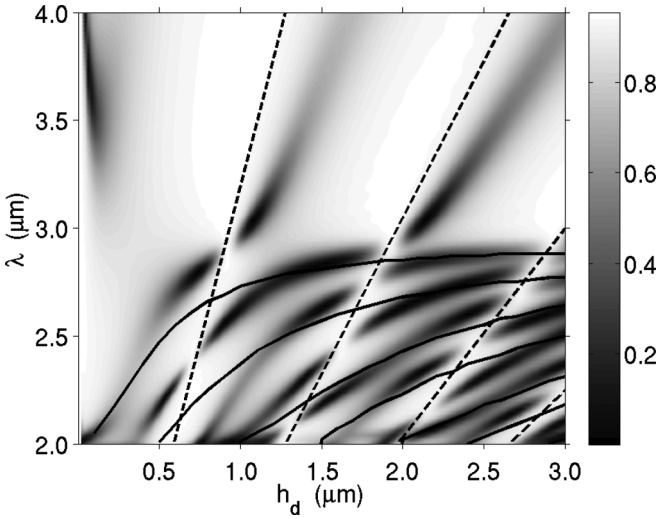

FIG. 8. Comparison of dispersion of TM and TE MIM waveguide modes with the reflectivity spectra of Fig. 2. The modes at $Q = 2\pi/a$ are drawn as solid lines. The modes alternate between TM and TE symmetry, with the one with the longest wavelength being TM. The dashed lines are from Eq. (10) using $\delta = 100$ nm.

the dielectric waveguide, along with the simulation results of Fig. 2. The agreement is not as good as for the cases with a 1D stripe array in Figs. 6 and 7, but we do now seem to have accounted for the appropriate number of resonances. There are also resonances associated with $Q = 0$ excitations. These are more evident for $\lambda > 3\ \mu$m, but their presence for shorter wavelengths may be inferred from the avoided crossings. Lastly, we remark that Eq. (10) is still doing well locating high R bridges.

To summarize, we have shown how one can understand the absorption resonances in a certain class of plasmonic nanostructures. Both the h_d dispersion of the resonances and their occasional, brief suppression can be explained by considering the behavior of systems with uniform layers. We acknowledge that our theory does depend on special conditions. In particular, we considered only light incident along the surface normal. Going to oblique incidence causes many of the resonances to split and leads to nontrivial polarization dependencies. We also examined only wavelengths above the diffraction threshold. This avoids the complication of multiple reflected beams at a given λ. However, we have in additional simulations found that the novel bridging phenomenon, described by Eq. (10), persists even with these complications, which lead to many new absorption channels.

We end by presenting in Fig. 9 an alternate view of the bridging effect for the case examined in Figs. 2 and 8. Over the range of h_d considered, only two resonances have $\lambda > a$. The one at longer wavelength shifts and strengthens as h_d increases, while the other also shifts but has its strength completely suppressed for h_d near 0.7 μm. The net result is that separation of the long-wavelength resonance from any other absorption structure is nearly doubled over a small range of h_d. From the absorption curve for $h_d = 0.7\ \mu$m we obtain that the fractional full width at half maximum is $\Delta\lambda/\lambda = 4\%$ for the resonance at $\lambda = 2.77\ \mu$m. This is significantly sharper than what is produced by the trapped plasmons at small h_d. Explicitly, when $h_d = 40$ nm, the trapped

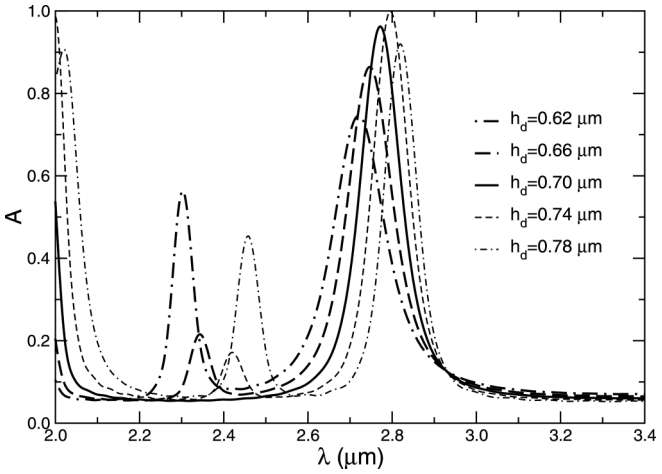

FIG. 9. Absorption spectra for light at normal incidence on the 2D array of round patches treated in Fig. 2. Note that the short-wavelength resonance disappears when $h_d = 0.7\mu$m. Its profile does not distort; its amplitude just vanishes.

plasmon resonance is at $\lambda = 4.02\ \mu$m and has $\Delta\lambda/\lambda = 11\%$. Hence, it is more isolated but broader. There may be applications where a trade-off of less isolation for a narrower resonance could be desired. An example is when one needs nearly monochromatic emission to detect specific gasses, a capability with security and defense applications.

In addition, the strong absorption at multiple wavelengths might be useful for sensing adsorbed species, but one needs to quantify how much adsorbates can shift the resonant strengths and locations. Similarly, studies of field profiles on resonance would be useful to establish general trends for by how much and at what locations local fields are enhanced. In the few cases we have examined, the enhancements at a strong resonance (deep valley in Figs. 6–8) are comparable to those found for the trapped plasmons at small h_d.

*Corresponding author: schaich@indiana.edu

[1]J. J. Greffet and M. Nieto-Vesperinas, J. Opt. Soc. Am. A **15**, 2735 (1998).
[2]N. C. Panoiu and R. M. Osgood, Jr., Opt. Lett. **32**, 2825 (2007).
[3]C. M. Wang, Y. C. Chang, M. W. Tsai, Y. H. Ye, C. Y. Chen, Y. W. Jiang, Y. T. Chang, and S. C. Lee, Opt. Express **15**, 14673 (2007).
[4]I. Puscasu and W. L. Schaich, Appl. Phys. Lett. **92**, 233102 (2008).
[5]Y. H. Ye, Y. W. Jiang, M. W. Tsai, Y. T. Chang, C. Y. Chen, D. C. Tzuang, Y. T. Wu, and S. C. Lee, Appl. Phys. Lett. **93**, 033113 (2008).
[6]J. Le Perchec, Y. Desieres, and R. E. de Lamaestre, Appl. Phys. Lett. **94**, 181104 (2009).
[7]X. Liu, T. Starr, A. F. Starr, and W. J. Padilla, Phys. Rev. Lett. **104**, 207403 (2010).
[8]N. Liu, M. Mesch, T. Weiss, M. Hentschel, and H. Giessen, Nano Lett. **10**, 2342 (2010).
[9]J. Hao, J. Wang, X. Liu, W. J. Padilla, L. Zhou, and M. Qiu, Appl. Phys. Lett. **96**, 251104 (2010).
[10]T. W. Lee and S. K. Gray, Opt. Express **18**, 23857 (2010).
[11]R. Ameling, L. Langguth, M. Hentschel, M. Mesch, P. V. Braun, and H. Giessen, Appl. Phys. Lett. **97**, 253116 (2010).
[12]P. Jouy, Y. Todorov, A. Vasanelli, R. Colombelli, I. Sagnes, and C. Sirtori, Appl. Phys. Lett. **98**, 021105 (2011).
[13]P. E. Chang, Y. W. Jiang, H. H. Chen, Y. T. Chang, Y. T. Wu, L. D. C. Tzung, Y. H. Ye, and S. C. Lee, Appl. Phys. Lett. **98**, 073111 (2011).
[14]M. N. Abbas, C. W. Cheng, Y. C. Chang, M. H. Shih, H. H. Chen, and S. C. Lee, Appl. Phys. Lett. **98**, 121116 (2011).
[15]Z. H. Jiang, S. Yun, F. Toor, D. H. Werner, and T. S. Mayer, ACS Nano **5**, 4641 (2011).
[16]J. Hao, L. Zhou, and M. Qiu, Phys. Rev. B **83**, 165107 (2011).
[17]J. A. Mason, S. Smith, and D. Wasserman, Appl. Phys. Lett. **98**, 241105 (2011).
[18]X. Liu, T. Tyler, T. Starr, A. F. Starr, N. M. Jokerst, and W. J. Padilla, Phys. Rev. Lett. **107**, 045901 (2011).

[19]B. Zhang, Y. Zhao, Q. Hao, B. Kiraly, I.-C. Khoo, S. Chen, and T. J. Huang, Opt. Express **19**, 15221 (2011).
[20]A. Cattoni, P. Ghenuche, A. M. Haghiri-Gosnet, D. Decanini, J. Chen, J.-L. Pelouard, and S. Collin, Nano Lett. **11**, 3557 (2011).
[21]C. Wu, B. Neuner III, G. Shvets, J. John, A. Milder, B. Zollars, and S. Savoy, Phys. Rev. B **84**, 075102 (2011).
[22]A. Tittl, P. Mai, R. Taubert, D. Dregely, N. Liu, and H. Giessen, Nano Lett. **11**, 4366 (2011).
[23]K. Aydin, V. E. Ferry, R. M. Briggs, and H. A. Atwater, Nat. Commun. **2**, 517 (2011).
[24]C. Koechlin, P. Bouchon, F. Pardo, J. Jeck, X. Lafosse, J.-L. Pelouard, and R. Haidar, Appl. Phys. Lett. **99**, 241104 (2011).
[25]Y. Cui, J. Xu, K. H. Fung, Y. Jun, A. Kumar, S. He, and N. X. Fang, Appl. Phys. Lett. **99**, 253101 (2011).
[26]S. Chen, H. Cheng, H. Yang, J. Li, X. Duan, C. Gu, and J. Tian, Appl. Phys. Lett. **99**, 253104 (2011),
[27]J. Hendrickson, J. Guo, B. Zhang, W. Buchwald, and R. Sorel, Opt. Lett. **37**, 371 (2012).
[28]Y. Zhao, Q. Hao, Y. Ma, M. Lu, B. Zhang, M. Lapsey, I.-C. Khoo, and T. J. Huang, Appl. Phys. Lett. **100**, 053119 (2012).
[29]P. Bouchon, C. Koechlin, F. Pardo, R. Haidar, and J.-L. Pelouard, Opt. Lett. **37**, 1038 (2012).
[30]C.-W. Cheng, M. N. Abbas, C.-W. Chiu, K.-T. Lai, M.-H. Shih, and Y.-C. Chang, Opt. Express **20**, 10376 (2012).
[31]R. Ameling and H. Giessen, Laser Photonics Rev. (in press) (2012).
[32]A. Taflove and S. C. Hagness, *Computational Electrodynamics: The Finite-Difference Time-Domain Method* (Artech House, Boston, 2005).
[33]A. Vial, A. S. Grimault, D. Macias, D. Barchiesi, and M. Lamy de la Chapelle, Phys. Rev. B **71**, 085416 (2005).
[34]S. Collin, F. Pardo, and J.-L. Pelouard, Opt. Express **15**, 4310 (2007).
[35]M. Cardona, Am. J. Phys. **39**, 1277 (1971).
[36]M. Born and E. Wolf, *Principles of Optics* (Pergamon, New York, 1999).